RESEARCH ARTICLE

Application of TiO₂/ZnS as a nano photocatalyst for degradation of Acid Red 18 in aqueous media using a central composite design

*Aref Shokri*¹, Mahdi Sanavi Fard²*

¹Jundi-Shapur Research Institute, Jundi-Shapur University of Technology, Dezful, Iran

²Department of Chemical Engineering, Tafresh University, Tafresh, Iran

ARTICLE INFO

ABSTRACT

In this study, through the application of TiO_2/ZnS as a novel nano photocatalyst, the degradation of AR18 in synthetic wastewater was explored. The nano photocatalyst was synthesized by the co-precipitation method and characterized by Scanning electron microscopy (SEM), Fourier transfer infrared (FT-IR), and X-ray powder diffraction (XRD) techniques. The average size of ZnS/TiO_2 nano photocatalyst was 79nm. For experimental design and statistical analysis of each factor including AR18 concentration, pH, catalyst dosage, and treatment time on the degradation rate of AR18 (response) by Central Composite Design (CCD) was used. The analysis of variance (ANOVA) demonstrates a second-order regression model with R^2 = 0.9995, adjusted R^2=0.9991, and predicted R^2=0.9982 for the removal of AR18. The optimum conditions for each operating factor were as the following: AR18 concentration at 30 mg.L^{-1}, catalyst dosage at 1.2 g.L^{-1}, pH at 5, and treatment time at 120 min. In these conditions, the actual and predicted AR18 removal was 94% and, 93.07%, respectively.

How to cite this article

INTRODUCTION

Nowadays, numerous industries like cosmetics ink, leather, tannery, printing, papermaking textiles, and the like, are discharging a significant volume of wasted dye into the environment [1]. These days not only penetrate underground and surface water sources and make them contaminated but also generate different types of mutations and have carcinogenic effects on human beings [2]. Hence, the efficient elimination of azo dyes is one of the major issues in wastewater remediation processes. According to the reports, in dye industry every year, around 15% of the generated dyes are unused in dyeing and industrial processes [3]. In different ways, dyes are carried in an aqueous media, as a result, it is crucial to remove them from their sources [4].

Conventional wastewater remediation processes are typically inefficient to remediate different types of complex wastewaters that include a combination of persistent and non-biodegradable mixtures. As a result, recently, comprehensive studies were performed by the researchers who have focused on the improvement of novel methods for overcoming shortcomings of conventional wastewater treatment approaches besides providing the efficient remediation of such complex wastewater matrices. Between different methods, due to the excellent performance in the removal of broad ranges of refractory pollutants, Advanced Oxidation Processes (AOPs) have been the focus of attention. Mainly, they rely on the in-situ generations of the hydroxyl radical (OH·), which is a non-selective powerful oxidant. During this process, due to the reaction between hydroxyl radicals with target organic pollutants, they are converted to less toxic

---

* Corresponding Author Email: *aref.shokri3@gmail.com*

and easily biodegradable products or mineralized. This property can be attributed to the non-selective nature of hydroxyl radicals, which enable them to degrade a wide range of refractory organic contaminants. Among different branches of AOPs, the photocatalysis method is highly promising because of its remarkable potential for the efficient degradation of persistent contaminants [5,6].

In this context, because of the harmless, stable, and photoactive nature of zinc sulfide (ZnS) and titanium dioxide (TiO$_2$), they have been used as a semiconductor for a long time in the environmentally friendly catalysis area. Due to the nanoscale influence of semiconductors, compared with bulk materials, they possess various improved optical behaviors, shapes, and sizes which result in their application in many areas like photocatalysis, optoelectronics, and electronics [7]. Brookite, rutile, and anatase are different types of TiO$_2$ as a transition metal oxide which among them, only rutile forms a stable frame [8,9]. Due to the significant surface area and remarkable energy driven by photogenerated electrons, anatase demonstrates maximum photoactivity. The bandgap of brookite, rutile, and anatase is 2.96 eV, 3.02 eV, and 3.2 eV, respectively [10]. High photoactivity, photochemical stability, non-toxic nature, and eco-friendliness are some of the major attractive features of titanium dioxide nanoparticles [11]. They have different utilizations in solar cells, electrochemical electrodes, temperature-sensing devices, ultra-thin capacitors, and photovoltaic cells [12]. Wurtzite (hexagonal form, bandgap of 3.91 eV) and Sphalerite (cubic structure, bandgap of 3.54 eV) are two polymorphs of zinc sulfide [13]. Nevertheless, the major downside of the application of TiO$_2$ particles in removal of azo dyes is challenging reusability, separation, agglomeration, and coagulation of TiO$_2$ nanoparticles. Moreover, the broad bandgaps of zinc sulfide and titanium dioxide are considered as disadvantage because they have restricted their utilizations to the ultra-violet area of the electromagnetic spectrum (responsible for 4-5 % of the solar spectrum) and they possess substantial electron-hole recombination. Through a hydrothermal approach to preparing nanoscale coupled TiO$_2$/ZnS semiconductor, these disadvantages were remarkably decreased. Not only the particle size can be governed by varying the processing time and temperature but also this approach is low-cost and simple. In comparison with synthesized TiO$_2$-P25, zinc sulfide, and titanium

dioxide nanoparticles, improved morphological, electrical, and optical properties were demonstrated through the integration of TiO$_2$/ZnS nanocomposite using the precipitation and sol-gel techniques. Also, using TiO$_2$/ZnS nanocomposite, the photodecomposition of phenol red sodium salt was quite efficient [14]. Through changing the molarity of ZnO nanoparticles and utilizing the sol-gel technique, TiO$_2$/ZnS nanocomposite was synthesized by Prasannalakshmi et al. [15]. According to the literature, the synthesis of TiO$_2$/ZnS nanocomposite was predominantly performed by the sol-gel technique. Priya et al. reported photodegradation of crystal violet dye using TiO$_2$/ZnS nanocomposite by the one-step hydrothermal method [16].

For exploring the significant variables in the AR18 removal, the OFAT (one factor at a time) strategy is inefficient. This is because not only the interactions between factors and their potential effect on each other are not calculated but also it is more complex, time-consuming, and cost-prohibitive [17] and the attempts must be intensified, especially when several parameters are required to be studied. In addition, for the optimization of factors, the OFAT results will not be reliable. Hence, this strategy is not economically feasible. To overcome this disadvantage and better optimization of AR18 removal, Response Surface Methodology (RSM) was used [18,19]. The RSM is a series of statistical methods which is beneficial for the analysis and modeling of problems in that a response of interest is heavily influenced by various factors, and the goal is to optimize of the target response [20]. One of the most widely used classes of RSM is CCD, which provides a very efficient tool for exploring the interactions of parameters on each other and process optimization [21].

The application of a novel nano photocatalyst synthesized by the co-precipitation method is the novelty of this research. In this study, the TiO$_2$/ZnS nano photocatalyst was used for the degradation of AR18 in synthetic wastewater. The catalyst was characterized by FTIR, XRD, and SEM methods. The influence of operational factors including AR18 concentration, photocatalyst dosage, pH, and treatment time on the degradation of AR18 by TiO$_2$/ZnS nano photocatalyst was investigated.

EXPERIMENTAL
Martials and Apparatus
Acid Red 18, NaOH, and HCl were supplied

from the Merck Company in Germany. The stock solutions were prepared with distilled water. The nanoparticles of ZnS and TiO$_2$ (in Anatase 30-70 nm) were procured from the Research Organization of Petroleum Manufacturing in Iran. The AR 18, as a utilized dye, was acquired from the Alvan Sabet Company in Iran, and its characteristics are presented in Table 1.

The XRD of the synthesized nanoparticle was logged in a 2θ range from 10°to 80° through Philips PW 1830 diffractometer as a high-resolution X-Ray Diffractometer with Cu-Kα radiation at λ = 1.54°A.

The FT-IR spectra in the form of KBr pellets were logged through Perkin–Elmer Spectrum GX FT-IR spectrometer as an Alpha-Bruker FT-IR spectrophotometer.

The SEM images were reserved by a German scanning electron microscope, LEO 1430 VP Carl Zeiss.

The Perkin Elmer UV-Vis Lambda 25 was used as a UV-Vis spectrophotometer for logging the spectra and calculating the absorbance of the dye at various operating intervals.

Synthesizing TiO$_2$/ZnS Nanocomposite

The chemicals used are of analytical grade without any additional purification and supplied from Sigma-Aldrich. The synthesizing procedure of TiO$_2$/ZnS nanoparticles is explained utilizing a schematic diagram (see Fig. 1). In a characteristic synthesis method, about 0.46 g of thioacetamide was added to 2 g of zinc nitrate hexahydrate (Zn (NO$_3$)$_2$.6H$_2$O) solution in 40 mL ethanol and the blended solution was stirred for 30 min at room temperature. The mix was transported into an autoclave with 100 mL capacity and heated at 100°C for 12 h. Through centrifugation, the subsequent deposition was recovered and washed with ethanol and distilled water for some time to eliminate the remaining ions. The resulting product was dried at 500°C for 8 h.

General Procedure

The photodegradation of AR18 using TiO$_2$/ZnS was conducted in a batch system at room temperature. The concentration of residual dye was obtained by absorbance measurement at 505 nm, using a UV-VIS spectrophotometer. The removal percentage of AR18 was calculated by the subsequent equation (Eq.1):

$$\text{AR18 removal (\%)} = \left(\frac{\text{AR18}_0 - \text{AR18}_t}{\text{AR18}_0}\right) \times 100 \quad (1)$$

Where AR18$_0$ and AR18$_t$ are the concentrations of AR18 at the start of the reaction and at time t, respectively.

Experimental Design

In the present study, the influence of four independent variables including AR18 concentration (A), catalyst dosage (B), pH (C), and treatment time (D) on the removal of AR18 (%) as the response by TiO$_2$/ZnS nano photocatalyst and application of CCD were explored. Each parameter was investigated in 5 levels. Table 2 presents the matrix of experimental elements and their values.

The following model (Eq. 2) was fitted in the form of a polynomial equation to the response variable (Y):

$$Y = \beta_0 + \sum_{j=1}^{k} \beta_j X_j + \sum_{i=1}^{k} \sum_{i=1}^{i<j} \beta_{ij} X_i X_j + \sum_{j=1}^{k} \beta_{jj} X_j^2 + \varepsilon \quad (2)$$

Where Y and k represent the response value, the number of independent variables, β$_0$ is constant-coefficient, X$_i$ … X$_k$ is coded independent parameters, β$_{jj}$ is the coefficient of the first-order or linear effect, β$_{jj}$ is the coefficient of quadratic or squared effect, and β$_{ij}$ is presenting the coefficient of interactions effect and e is the random error account for any discrepancy or uncertainty between predicted and real value. Table 3 presents design points, including 4 major parameters and response values.

RESULTS AND DISCUSSION

Characterization of TiO$_2$/ZnS nano photocatalyst FT-IR Spectra Analysis

The FT-IR (Shimadzu Irtracer-100) was applied to ascertain the different functional groups of the sample.

The FT-IR spectra of the ZnS coupled TiO$_2$ nanocomposite has been presented in Fig. 2. The wideband positioned at 500–600 cm^{-1} is allocated to the vibration of the TiO bonds. The vibration peak of ZnS is characterized at around 1100 cm^{-1} [22] that is without pure TiO$_2$, which approves the existence of ZnS in the structure of ZnS/TiO$_2$. It should be noted that the wide peaks seeming at 3100–3600 cm^{-1} and the robust bands at 1615–1635 cm^{-1} originated from the hydroxyl group of H$_2$O molecules adsorbed to the surface of ZnS/TiO$_2$ nano photocatalyst.

Table 1. Chemical properties of AR18.

Dye name	Chemical structure	λ$_{max}$(nm)	Molecular Mass
Acid Red 18 (C$_{20}$H$_{11}$N$_2$Na$_3$O$_{10}$S$_6$)		505	604.48
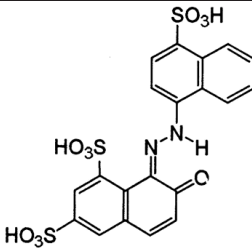
Table 2. Level and ranges of each factor.

Variables	Code	Range and levels				
		−α	-1(Low)	0 (Middle)	+1(High)	+α
AR18 concentration (mg. L^{-1})	A	20	30	40	50	60
Catalyst dosage (g.L^{-1})	B	0.3	0.6	0.9	1.2	1.5
pH	C	3.0	5	7	9	11
Treatment time (min)	D	30	60	90	120	150
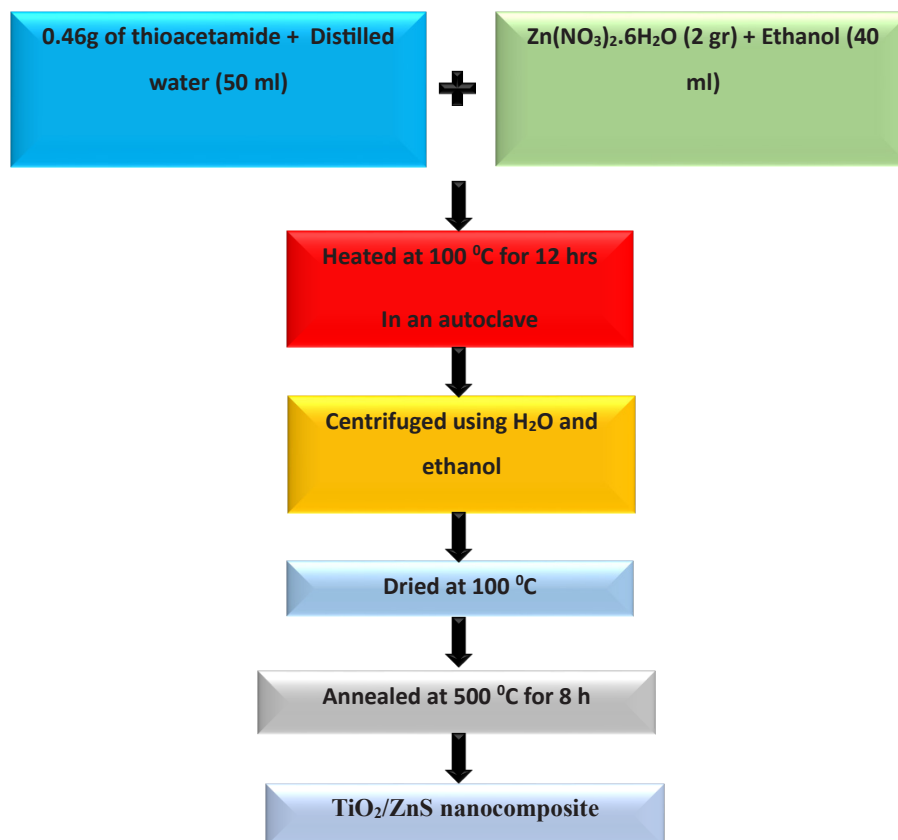
Fig. 1. The synthesizing process of TiO$_2$/ZnS nanocomposite.

Table 3. CCD results of four independent variables and AR18 removal (%).

Run No.	AR18 concentration	Catalyst dosage	pH	Treatment time	AR18 Removal (%)
	Factors				Response
1	30	1.2	9	120	74.7
2	40	0.9	7	30	18
3	40	1.5	7	90	64
4	50	0.6	9	60	18
5	40	0.9	7	90	48
6	40	0.9	3	90	58
7	50	0.6	5	60	21
8	50	1.2	9	120	49
9	40	0.9	7	90	48.4
10	40	0.9	11	90	36.3
11	50	1.2	5	60	38
12	40	0.9	7	90	48.7
13	40	0.3	7	90	19
14	50	1.2	5	120	64.5
15	30	1.2	9	60	45
16	50	0.6	5	120	38
17	30	0.6	9	60	25.5
18	30	0.6	5	60	33.5
19	50	1.2	9	60	27.2
20	30	1.2	5	60	59
21	30	0.6	9	120	46.4
22	20	0.9	7	90	67
23	30	1.2	5	120	93.2
24	40	0.9	7	90	47.1
25	50	0.6	9	120	29
26	40	0.9	7	150	64
27	40	0.9	7	90	47.5
28	30	0.6	5	120	57.8
29	40	0.9	7	90	47.5
30	60	0.9	7	90	30.3
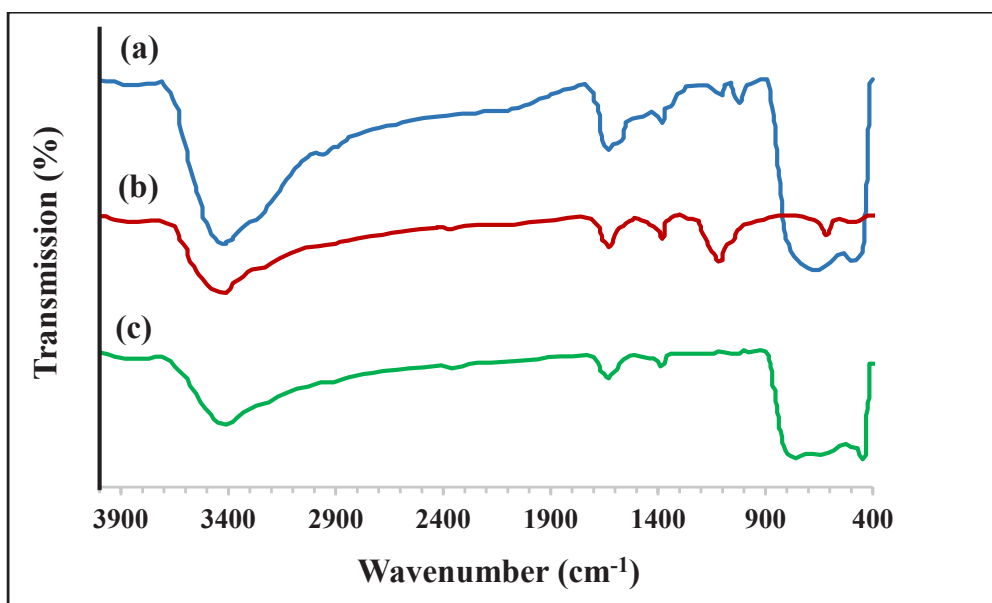
Fig. 2. FT-IR spectra of (a) ZnS/TiO$_2$, (b) ZnS, and (c) TiO$_2$ nano photocatalyst.

(a)

(b)

(c)
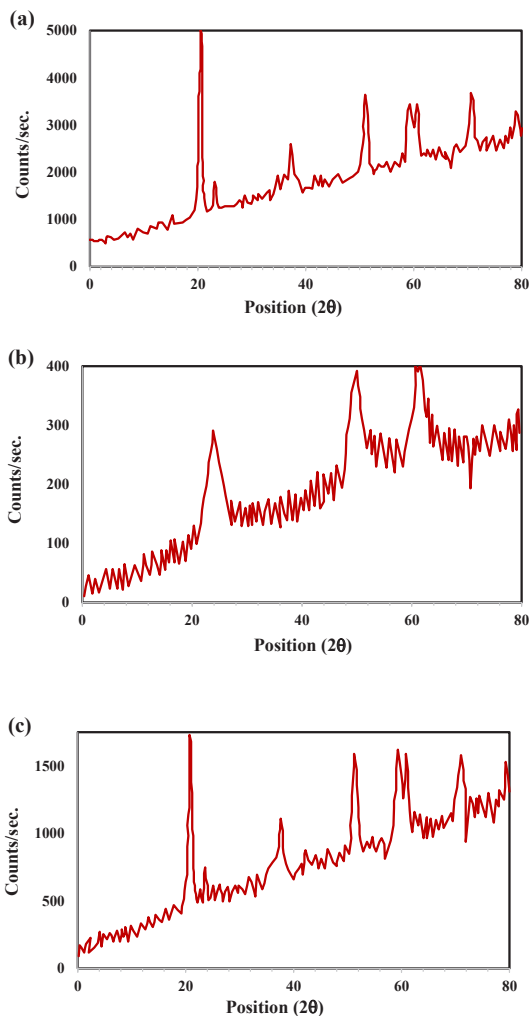
Fig. 3.a, b, c. The XRD patterns of (a) TiO_2, (b) ZnS and (c) ZnS/ TiO_2 nano photocatalyst.

XRD Analysis

The powder X-ray diffraction (XRD) analysis was performed by Bruker D8 advanced XRD system. The Cu ka radiation of wavelength 1.5406 A° was utilized as an X-ray source in the sample. The crystallite size of the particle was measured by Scherrer's equation.

The XRD patterns of the TiO_2, ZnS, and attained ZnS/TiO_2 samples are represented in Fig. 3. The XRD patterns of the pure ZnS (Fig. 3b) displayed the typical reflection plans (310), (220), and (110) that can be related to the cubic phase of ZnS [23]. It is obvious that in the diffraction pattern of ZnS/TiO_2 the intensity of the peaks related to the nanoparticles of ZnS was inferior to pure nano ZnS. Thus, the XRD characterization did not establish related peaks of ZnS after the deposition

on the TiO_2 surfaces (Fig. 3c). In ZnS/TiO_2 sample, the expansion of the XRD peaks of ZnS can be related to the small quantity and poor crystallinity of existing ZnS in the sample and the small size and high crystallinity of the TiO_2 [24]

To detect the presence of zinc sulfide and titanium dioxide nanoparticles in the sample, analyzing crystallite size, phase identification, and crystal structure, the XRD pattern was utilized. The crystal phases were detected with 2q values varying from 10 to 80^0.

Utilizing Scherrer's equation (Eq.3), the average crystallite size of TiO_2/ZnS nanoparticle was calculated:

$$D = \frac{K\lambda}{\cos\theta \beta_{hkl}} \qquad (3)$$

Where K is the dimensionless shape factor that is equal to 0.9, β_{hkl} β_{hkl} is the full-width half-maximum of the various peak, k is the wavelength of Cu Ka radiation and q is the diffraction angle. The Scherrer's equation is just utilized to detect the crystallite size of the nanoparticle and because of decreased crystallite size, it will not regard the lattice strain that happens in the sample [25]. The average size of ZnS/TiO_2 nano photocatalyst was 79nm.

SEM Images

The SEM was utilized to establish the surface morphology of the catalyst. The distinctive morphology and size of the achieved ZnS/TiO_2 nano catalyst were achieved by SEM. The results are shown in Fig. 4. The morphological modifications of ZnS/TiO_2 heterostructure are detected via SEM images. The flower-like ZnS particles are entirely deposited on TiO_2. The morphology is like those stated by other researchers previously [7].

The Analysis of Variance (ANOVA)

The current study explores the effect of 4 independent variables on the response using CCD to determine optimum operating conditions. The major statistical values of each variable are shown in Table 4. Based on the results of the ANOVA, the F-value of 2299.72 confirmed that the model is highly robust toward the effect of noise. In other words, the feasibility of such a large F-value due to noise to occur is only 0.01%. According to the statistical standards and as suggested by Design-Expert software, the factors that have P values equal to or less than 0.05 are considered significant. In this case, A, B, C, D, AC, AB, AD, BD, BC, B²,

Table 4. ANOVA results for the removal of AR18 using TiO$_2$/ZnS nano photocatalyst.

Source	Sum of Squares	df	Mean Square	F-value	p-value	Percent Contribution (%)
Model	9564.04	14	683.15	2299.72	< 0.0001	Significant
A-AR18 Dosage	2086.94	1	2086.94	7025.40	< 0.0001	21.82
B-Catalyst	3069.08	1	3069.08	10331.68	< 0.0001	32.09
C-pH	743.71	1	743.71	2503.59	< 0.0001	7.77
D-Treatment Time	3206.28	1	3206.28	10793.54	< 0.0001	33.52
AB	81.00	1	81.00	272.68	< 0.0001	0.85
AC	11.56	1	11.56	38.92	< 0.0001	0.12
AD	67.24	1	67.24	226.35	< 0.0001	0.7
BC	46.92	1	46.92	157.96	< 0.0001	0.49
BD	95.06	1	95.06	320.02	< 0.0001	1
CD	21.62	1	21.62	72.79	< 0.0001	0.22
A^2	1.92	1	1.92	6.46	0.0225	0.02
B^2	63.61	1	63.61	214.15	< 0.0001	0.66
C^2	0.3344	1	0.3344	1.13	0.3055	0.003
D^2	74.49	1	74.49	250.75	< 0.0001	0.78
Residual	4.46	15	0.2971			100.0
Lack of Fit	2.60	10	0.2603	0.7021	0.7041	Not Significant
Pure Error	1.85	5	0.3707			
Cor Total	9568.49	29				

Model Summary

R^2	0.9995	Standard Dev.	0.5450
Adjusted R^2	0.9991	Mean	45.45
Predicted R^2	0.9982	C.V %	1.20
Adequate Precision	195.9472		
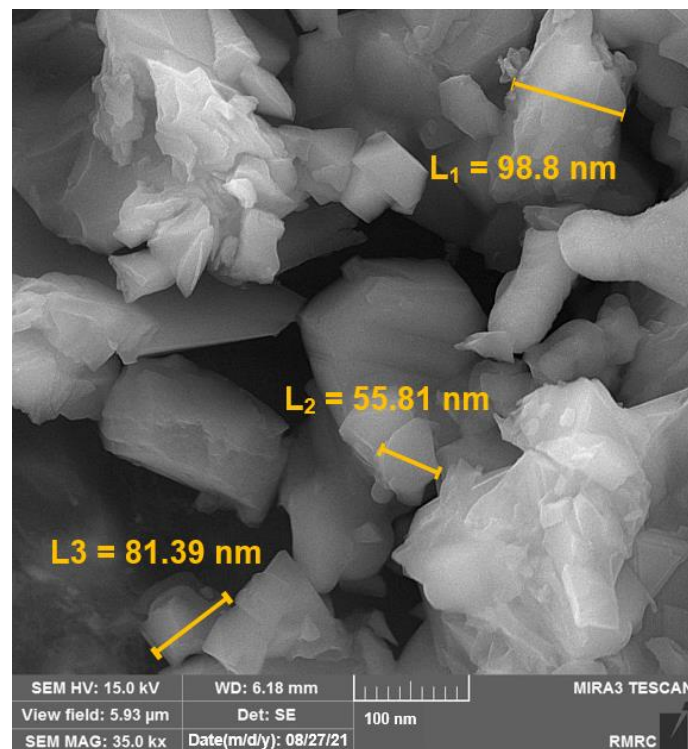
Fig. 4. SEM images of ZnS/TiO$_2$ nano photocatalyst.
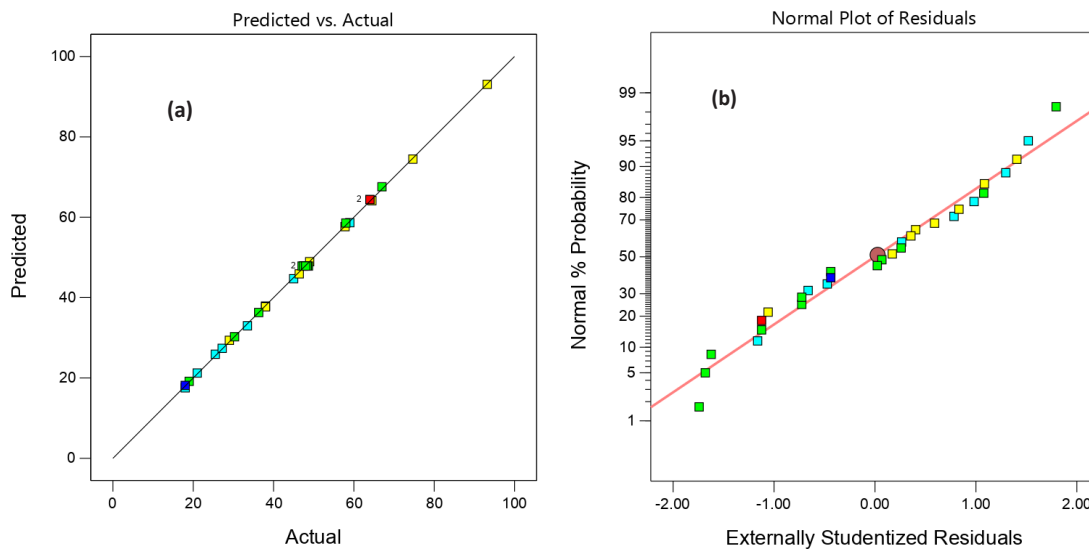
Fig. 5. (a) Comparison between predicted and experimental values for the removal of the AR18 using TiO$_2$/ZnS nano photocatalyst, (b) Normal probability diagram for the model.

CD, A², and D² are in significant model terms. The "Lack of Fit" is the amount that the model predictions miss the observations. It is measured by comparing pure error with residual error from the replicated design points, which typically are the central points in the experiment. If the lack of fit value goes beyond F-value, it is indicated that there is a fault with the lack of fit, and as a result, the regression model needs enhancement. To end this, the lack of fit F-value of 0.7041 indicates the lack of fit is not significant compared to the pure error, and the possibility of occurring such a large lack of fit F-value is 70.41% because of noise. Always, an insignificant lack of fit values is desirable.

The correlation between factors and the AR18 removal (%) in terms of coded factors are presented in Eq. 4:

$$\text{Removal of AR18 (\%)} = +47.87 - 9.32A + 11.31B - 5.57C + 11.56D - 2.25AB + 0.85AC - 2.05AD - 1.71BC + 2.44BD - 1.16CD + 0.2646A^2 - 1.52B^2 - 0.1104C^2 - 1.65D^2 \qquad (4)$$

To predict response values for a given level of each variable, the coded equation can be used. The low and high levels of each variable are coded by -1 and +1, respectively. By comparing each factor in coefficient, the related influence of each factor on the response can be determined [17]. As it is obvious from the coefficient of variation in the coded equation, time is the most influential factor in the removal of AR18. The coefficient of

determination or R squared (R²) is explained as the amount of variation in the data described by the ANOVA model [17]. In other words, it is a statistical estimation of how close the experimental data are to the fitted regression line. As a result, according to its value, the model explains almost a total of the variability in the experiment. The adjusted R² is a deviation of the R² statistics that reflects the number of model factors [17]. The predicted R² and adjusted R² are between 0.9982 and 0.9991, respectively which indicates reasonable agreement between them because their difference is less than 0.2. Adequate precision is defined as the signal-to-noise ratio. Large values of adequate precision are desirable, and values that exceed 4 usually indicate that the model will give enough performance in prediction. Hence, the ratio of 195.9472 demonstrates an appropriate signal which means that the model can be applied to the navigation of the design space.

According to Fig. 5a, the actual and predicted results are close enough together and the precision of the regression model is confirmed. The normal probability plot implies whether the residuals track the straight line and normal distribution or not. As it is clear from Fig. 5b, the experimental data are distributed evenly on a straight line as a result the underlying assumption of statistics regarding normality is validated.

For determination of the effect of each operative factor on the response, the percent of contribution

Pareto Chart

	Percent Contribution
0.78	Time^2
0.003	pH^2
0.66	Catalyst^2
0.02	AR18^2
0.22	(pH*Time)
1	(Catalyst*Time)
0.5	(Catalyst*pH)
0.7	(AR18*Time)
0.12	(AR18*pH)
0.85	(AR18*Catalyst)
33.5	Time
7.75	pH
32.1	Catalyst
21.8	AR18

Percent Contribution of Each Term
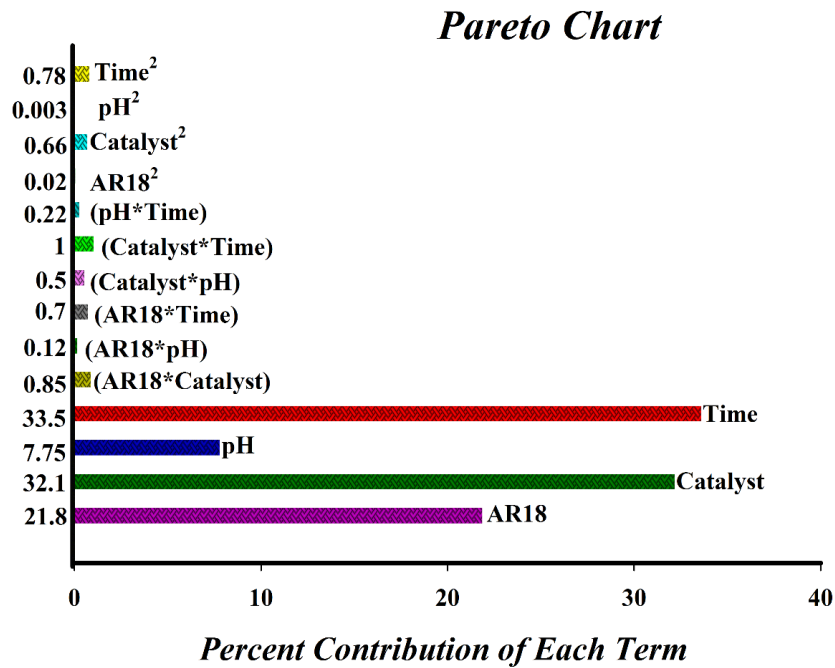
Fig. 6. Graphical Pareto chart for AR18 removal.

was calculated by Eq.5 and presented as the Pareto chart (See Fig. 6).

$$P_i \ (\%) = \left(\frac{b_i^2}{\sum b_i^2}\right) \times 100 \qquad (5)$$

The term b_i indicates the effect of the numerical coefficient for each factor. The time and concentration of catalyst remarkably affect the removal of AR18 compared with the other variables.

Effect of AR18 Concentration

The influence of AR18 concentration on the degradation of AR18 using TiO$_2$/ZnS nano photocatalyst was illustrated in Fig. 7. It is evident that increasing the concentration of AR18 decreases the removal percentage of AR18. The reason is that with increasing dosage of AR18 higher numbers of its molecules were reacted with accessible active sites of catalyst and the mineralization rate increased. However, extreme concentration of AR18 filtering irradiated light photons and reduced the generation rate of hydroxyl radicals and therefore remarkably reducing the degradation rate of AR18.

Effect of Catalyst amounts

The effect of photocatalyst amount on the elimination of AR18 using TiO$_2$/ZnS is demonstrated in Fig. 8, which is evident they are directly proportional together. The reason is that in the higher concentration of catalysts, the active sites on the surface of the catalyst were enhanced to get more photons, which leaded to the generation of more hydroxyl and superoxide radicals, and accordingly, more AR18 molecules degraded. Several studies report that the degradation of tartrazine and methylene blue are amplified by increasing the catalyst concentration. Since the number of active sites was enhanced with rising catalyst concentration and more photons were adsorbed, and following that, more superoxide and hydroxyl radicals were generated, causing more contaminant mineralization [26]. Also, this finding is promising for the works of Shokri and Karimi [27] who studied the degradation of AR18 using TiO$_2$/zeolite nano photocatalyst.

Effect of pH

The influence of pH on the degradation of AR18 was demonstrated in Fig. 9. The solution pH is a crucial aspect in the photocatalytic method since it heavily influences the chemistry of the pollutant molecule and the surface charge of the catalyst and as a result, the interaction between the adsorbent and the adsorbate. Hence, the sorption of AR18 on TiO$_2$/ZnS nano photocatalyst was
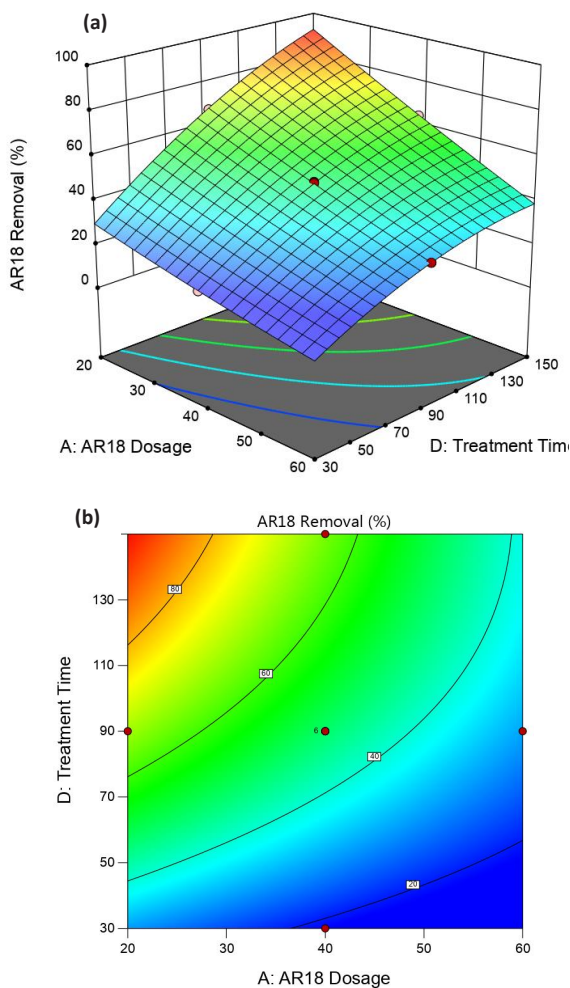
Fig. 7 (a) 3D and (b) contour plots for the effect of AR18 concentration on the degradation of AR18.
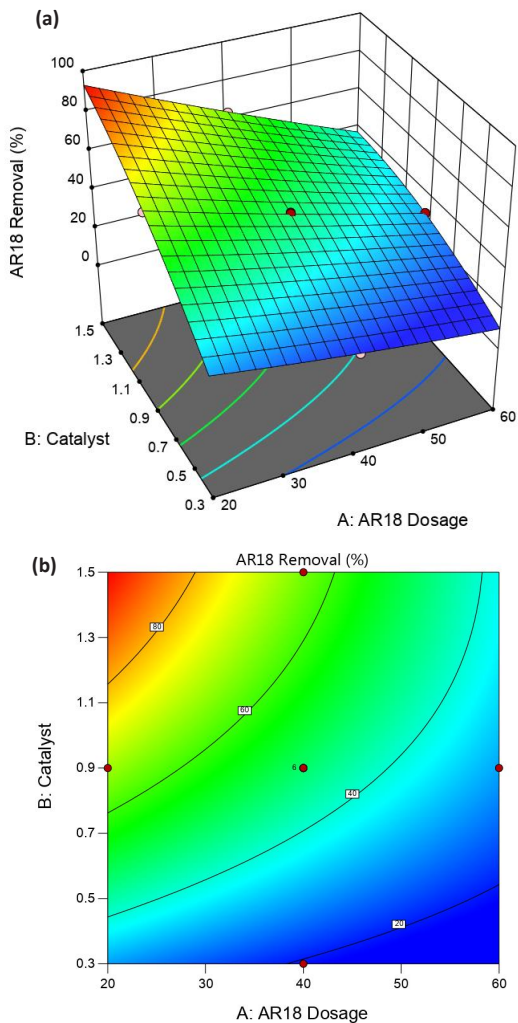
Fig. 8 (a) 3D and (b) contour plots for the influence of catalyst dosage on the degradation of AR18.

conducted with various pH values from 3 to 11. At acidic pH values, the removal of AR18 was higher which can be attributed to the ZnS capability to produce hydrogen bonding with hydronium ions which causes the anionic dye to be adsorbed on the positive surface of nano TiO$_2$/ZnS. The significant decrease of sorption at alkaline pH values might stem from the hydroxyl ions gathering on TiO$_2$/ZnS surface and subsequent electrostatic repulsion between anionic dye and negatively charged adsorbent.

Also, the pH had a negative effect on the elimination of AR18 and it was increased by falling pH. The removal of AR18 was improved in the low pH, due to the robust electrostatic adsorption of amid, the positive charge of the catalyst and the negative charge of the pollutant. Hence, the attractive forces between the catalyst and AR18

molecules causing AR18 photodegradation were raised [28].

The photodegradation of MC-LR by nano photocatalyst of Ag/AgCl/TiO$_2$ was studied by Liao et al., and the degradation efficiency was amplified with reducing in the initial pH, because of the attractive forces between the catalyst and contaminant molecules [29]. Moreover, a similar study revealed that the removal of Direct Red 16 was decreased in an alkaline environment. Because, in acidic media, with electrostatic force between the dye molecules and catalyst surface, the photocatalytic activity was enhanced [30].

Influence of Treatment Time
The effect of treatment time on the AR18 using TiO$_2$/ZnS photocatalyst at a catalyst dosage of 0.9 and pH 7 was presented in Fig. 10. As it is

119

(a)

(a)

(b)

(b)
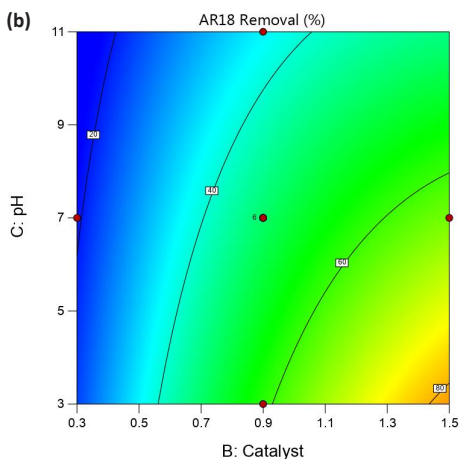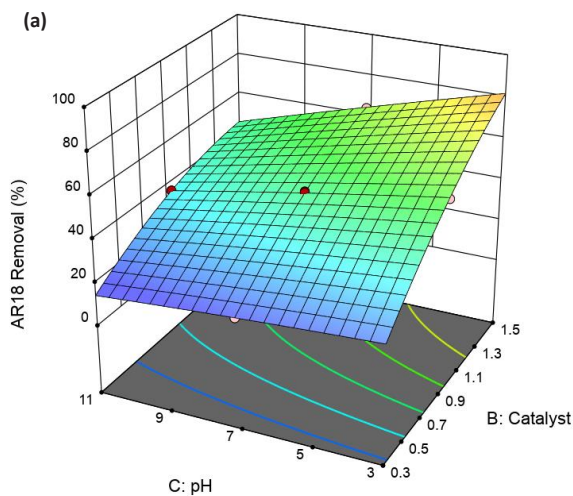
Fig. 9 (a) 3D and (b) contour plots for the effect of pH on the degradation of AR18.
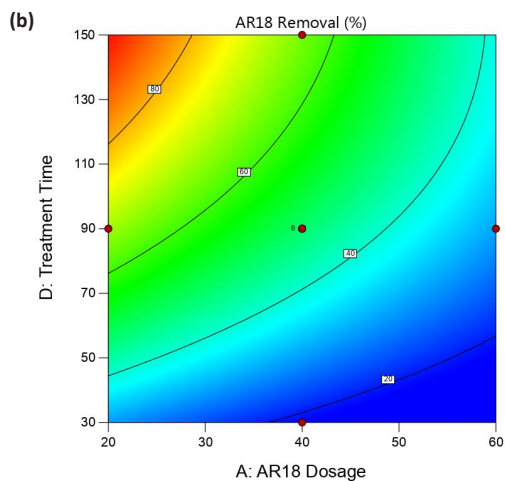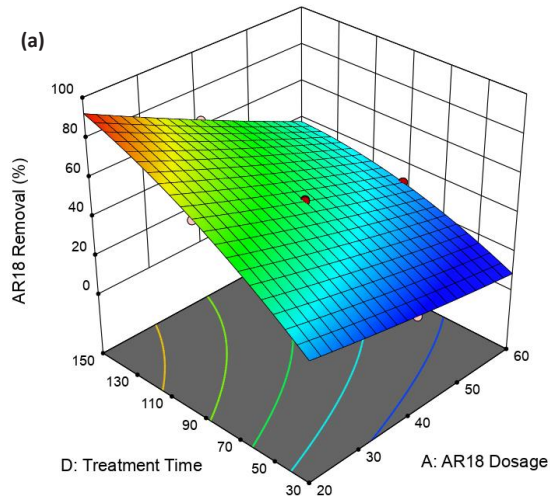
Fig. 10. (a) 3D and (b) contour plots for the effect of treatment time on the degradation of AR18.

evident, after 150 min, the mineralization of AR18 was increased to its highest degree. The outcomes confirmed that there is a positive correlation between treatment time and AR18 degradation. As a result, the elimination performance of AR18 was improved by increasing treatment time. This is because by enhancing the treatment time, the feasibility of the interaction between AR18 molecules and the electron-hole pair is enhanced. This result is promising to the works of Shokri and Karimi [27] who studied the degradation of AR18 using TiO₂/zeolite nano photocatalyst. Moreover, based on the investigations of Rahimi et al., with increasing treatment time the higher quantity of Acid Orange 10 was degraded in a way that it was increased from 0% to 94% from the initial time of reaction to 150 min [28]. Other scholars reported

that the elimination effectiveness of Direct Blue 71 and tartrazine was directly proportional to treatment time since the active sites of photocatalyst on the catalyst surface were enhanced with an increase in the treatment time [31].

Response Optimization and Validation

Exploring the optimum conditions of each parameter to obtain the highest rate of AR18 removal using TiO₂/ZnS nano photocatalyst was the primary goal of the present study. These optimum conditions are presented in Table 5. To validate them, further experimental tests were conducted. Based on the results, when the quantity of each factor was set at the optimum values, the maximum removal of AR18 was achieved, which was in enough agreement with the values predicted

Table 5. Optimum operational conditions for maximum removal of AR18 (%).

Variables	Optimum values for the removal of AR18 (%)
AR18 Concentration	30
Catalyst dosage	1.2
pH	5
Treatment time	120
Removal of AR18 (%)	Prediction (93.07), Experimental (94%)

by the regression model. As a result, it can be concluded that CCD can yield highly satisfactory results and can be applied as a reliable method for the investigation of the best-operating conditions.

CONCLUSION

In the current study, the efficiency of TiO₂/ZnS nano photocatalyst was explored for photodegradation of AR18 in synthetic wastewater using CCD. The synthesized TiO₂/ZnS was produced by the co-precipitation way and characterized by the SEM, FT-IR, and XRD techniques. The effect of 4 critical variables including AR18 concentration, catalyst dosage, pH, and treatment time on the removal of AR18 has been studied. The predicted optimal conditions by the model were as the following: AR18 concentration = 30 mg. L⁻¹, catalyst dosage = 1.2 g. L⁻¹, pH =5 and treatment time = 120 min. In these conditions, as predicted by the model, the highest percentage of AR18 removal was 93.07. The ANOVA results presented a highly satisfactory second-order regression model for the removal of AR18. The high determination coefficient quantities (R^2=0.9995, predicted R^2=0.9982, and adjusted R^2=0.9991) confirmed the reliability of the model. To interpret the influence of each parameter besides their interactions on each other, the counter and the 3D plots were used. The mechanism of catalyst in the degradation of AR18 was explained. The results showed that TiO₂/ZnS nano photocatalyst is a promising and efficient method for AR18 degradation.

CONFLICT OF INTEREST

The authors declare no conflicts of interest.

REFERENCES

[1] M. Soniya, G. Muthuraman, Int. J. ChemTech Res. 7: 3046 (2015).

[2] R.O. Alves de Lima, A.P. Bazo, D.M.F. Salvadori, C.M. Rech, D. de Palma Oliveira, G. de Aragão Umbuzeiro, Mutat. Res. - Genet. Toxicol. Environ. Mutagen. 626: 53 (2007). https://doi.org/10.1016/j.mrgentox.2006.08.002.

[3] A.Shokri, Chemosphere, 296:133817(2022)https://doi.org/10.1016/j.chemosphere.2022.133817

[4] H.R. Rajabi, H. Arjmand, S.J. Hoseini, H. Nasrabadi, J. Magn. Magn. Mater. 394: 7 (2015). https://doi.org/10.1016/j.jmmm.2015.06.024.

[5] A.Shokri, Environ. Chall., 5:100332(2021). https://doi.org/10.1016/j.envc.2021.100332

[6] A. Shokri, M. Abdolkarimi, F. Soleimani, J. Nanoanalysis. 0: (2022). https://doi.org/10.22034/JNA.2022.1934052.1262.

[7] S. Talebi, N. Chaibakhsh, Z. Moradi-Shoeili, J. Appl. Res. Technol. 15: 378 (2017). https://doi.org/10.1016/j.jart.2017.03.007.

[8] Y. Fang, C. Xing, S. Zhan, M. Zhao, M. Li, H. Liu, J. Mater. Chem. B. 7: 1933 (2019). https://doi.org/10.1039/C8TB03331E.

[9] J. Jalali, M. Mozammel, J. Mater. Sci. Mater. Electron. 28: 5336 (2017). https://doi.org/10.1007/s10854-016-6192-8.

[10] G. Sharma, A. Kumar, S. Sharma, M. Naushad, R. Prakash Dwivedi, Z.A. ALOthman, G.T. Mola, J. King Saud Univ. - Sci. 31: 257 (2019). https://doi.org/10.1016/j.jksus.2017.06.012.

[11] J. Chen, C. Ning, Z. Zhou, P. Yu, Y. Zhu, G. Tan, C. Mao, Prog. Mater. Sci. 99: 1 (2019). https://doi.org/10.1016/j.pmatsci.2018.07.005.

[12] R. V. Nair, P.K. Gayathri, V.S. Gummaluri, P.M.G. Nambissan, C. Vijayan, J. Phys. D. Appl. Phys. 51: 045107 (2018). https://doi.org/10.1088/1361-6463/aaa187.

[13] P. Iranmanesh, S. Saeednia, M. Nourzpoor, Chinese Phys. B. 24: 046104 (2015). https://doi.org/10.1088/1674-1056/24/4/046104.

[14] N. Wetchakun, B. Incessungvorn, K. Wetchakun, S. Phanichphant, Mater. Lett. 82: 195 (2012). https://doi.org/10.1016/j.matlet.2012.05.092.

[15] P. Prasannalakshmi, N. Shanmugam, Spectrochim. Acta - Part A Mol. Biomol. Spectrosc. 175: 1 (2017). https://doi.org/10.1016/j.saa.2016.12.018.

[16] G.H. Priya, A.A. Shaly, J.M. Linet, J. Mater. Sci. Mater. Electron. 32: 5790 (2021). https://doi.org/10.1007/s10854-021-05300-2.

[17] Douglas C. Montgomery, Design and Analysis of Experiments, 10th Edition, Wiley, (2019).

[18] M. Ahmadi, F. Ghanbari, Environ. Sci. Pollut. Res. 23: 19350 (2016). https://doi.org/10.1007/s11356-016-7139-6.

[19] A. Shokri, Int. J. Ind. Chem. 9: 295 (2018). https://doi.org/10.1007/s40090-018-0159-y.

[20] A. Shokri, A. Bayat, K. Mahanpoor, Desalin. Water Treat. 166: 135 (2019). https://doi.org/10.5004/dwt.2019.24634.

[21] A.Shokri, Int. J. Env. Anal. Chem.102:5077(2022).https://doi.org/10.1080/03067319.2020.1791328

[22] X. Tian, J. Wen, S. Wang, J. Hu, J. Li, H. Peng, Mater. Res. Bull. 77: 279 (2016). https://doi.org/10.1016/J.MATERRESBULL.2016.01.046.

[23] A. Roychowdhury, S.P. Pati, S. Kumar, D. Das, Powder Technol. 254: 583 (2014). https://doi.org/10.1016/J.POWTEC.2014.01.076.

[24] K.K. Senapati, C. Borgohain, P. Phukan, Catal. Sci. Technol. 2: 2361 (2012). https://doi.org/10.1039/C2CY20400B.

[25] R.A. Faris, Iraqi J. Phys. 11: 64 (2019). https://doi.org/10.30723/ijp.v11i22.354.

[26] W. Liao, Y. Zhang, M. Zhang, M. Murugananthan, S. Yoshihara, Chem. Eng. J. 231: 455 (2013). https://doi.org/10.1016/j.cej.2013.07.054.

[27] A. Shokri, S. Karimi, J. Water Environ. Nanotechnol. 6: 326 (2021). https://doi.org/10.22090/jwent.2021.04.004.

[28] B. Rahimi, N. Jafari, A. Abdolahnejad, H. Farrokhzadeh, A. Ebrahimi, J. Environ. Chem. Eng. 7: 103253 (2019). https://doi.org/10.1016/j.jece.2019.103253.

[29] N. Arabzadeh, A. Mohammadi, M. Darwish, S. Abuzerr, J. Chinese Chem. Soc. 66: 474 (2019). https://doi.org/10.1002/jccs.201800302.

[30] N. Jafari, K. Ebrahimpour, A. Abdolahnejad, M. Karimi, A. Ebrahimi, J. Environ. Heal. Sci. Eng. 17: 1171 (2020). https://doi.org/10.1007/s40201-019-00432-4.

[31] A. Shokri, Desalin. Water Treat. 58: 258 (2017). https://doi.org/10.5004/dwt.2017.0292.